Ecosystem CO_2 Exchange and Its Economic Implications in Northern Permafrost Regions in the 21st Century

Cuicui Mu[1,2] , Xiaoxiao Mo[1], Yuan Qiao[1], Yating Chen[3] , Yuguo Wei[1], Mei Mu[1], Jinyue Song[1], Zhilong Li[1], Wenxin Zhang[4,5] , Xiaoqing Peng[1] , Guofei Zhang[1] , Qianlai Zhuang[6] , and Mika Aurela[7]

[1]Key Laboratory of Western China's Environmental Systems (Ministry of Education), College of Earth and Environmental Sciences, Observation and Research Station on Eco-Environment of Frozen Ground in the Qilian Mountains, Lanzhou University, Lanzhou, China, [2]Cryosphere Research Station on Qinghai-Tibetan Plateau, State Key Laboratory of Cryospheric Science, Northwest Institute of Eco-Environment and Resources, Chinese Academy of Sciences, Lanzhou, China, [3]College of Geography and Environment, Shandong Normal University, Jinan, China, [4]Department of Physical Geography and Ecosystem Science, Lund University, Lund, Sweden, [5]Center for Permafrost (CENPERM), Department of Geosciences and Natural Resource Management, University of Copenhagen, Copenhagen, Denmark, [6]Department of Earth, Atmospheric, and Planetary Sciences, Purdue University, West Lafayette, IN, USA, [7]Finnish Meteorological Institute, Helsinki, Finland

Abstract Climate warming increases carbon assimilation by plant growth and also accelerates permafrost CO_2 emissions; however, the overall ecosystem CO_2 balance in permafrost regions and its economic impacts remain largely unknown. Here we synthesize in situ measurements of net ecosystem CO_2 exchange to assess current and future carbon budgets across the northern permafrost regions using the random forest model and calculate their economic implications under the Shared Socio-economic Pathways (SSPs) based on the PAGE-ICE model. We estimate a contemporary CO_2 emission of 1,539 Tg C during the nongrowing season and CO_2 uptake of 2,330 Tg C during the growing season, respectively. Air temperature and precipitation exert the most control over the net ecosystem exchange in the nongrowing season, while leaf area index plays a more important role in the growing season. This region will probably shift to a carbon source after 2,057 under SSP5-8.5, with a net emission of 17 Pg C during 2057–2100. The net economic benefits of CO_2 budget will be $4.5, $5.0, and $2.9 trillion under SSP1-2.6, SSP2-4.5, and SSP5-8.5, respectively. Our results imply that a high-emission pathway will greatly reduce the economic benefit of carbon assimilation in northern permafrost regions.

Plain Language Summary The permafrost regions account for approximately 22% of the land area in the northern hemisphere. The soil organic carbon stored in permafrost is about twice as much as currently contained in the atmosphere. Once permafrost thaws, the soil organic carbon will be utilized by microbes, and large amounts of CO_2 will be released, further accelerating climate warming. On the other hand, warming significantly promotes vegetation growth and makes more carbon to be absorbed. The current and future carbon balance in northern permafrost regions remains largely unknown. Here, we calculated the carbon budget based on in situ observations of CO_2 flux. Our results provide a deep insight into understanding how much carbon has been assimilated and released in northern permafrost ecosystems. Our findings have important implications for the future role of northern permafrost in regulating the ecosystem carbon cycle and economic benefit.

1. Introduction

Northern permafrost regions contain approximately 1,460–1,600 Pg soil organic carbon(Schuur et al., 2022), and these regions will gradually shift from carbon sinks to carbon sources in this century (Miner et al., 2021; Turetsky et al., 2020). Under high emission scenarios (RCP 8.5 in IPCC 5, A2 in IPCC4), soil organic carbon loss from permafrost thaw ranged from 9 to 140 Pg (1 Pg = 10^{15} g) carbon by 2100 (Burke et al., 2013; Deimling et al., 2012; Koven et al., 2011; Schaefer et al., 2011; Zhuang et al., 2006). Based on an expert assessment, the permafrost carbon loss was estimated at 120–195 Pg C by 2100 under the RCP 8.5 scenario (Schuur et al., 2013). An ensemble of 50 models projects CO_2 release from permafrost to be 3–41 Pg C per 1°C of global warming by 2100 (Masson-Delmotte et al., 2021). These studies highlighted the importance of permafrost-affected carbon and suggested that permafrost thaw will lead to considerable carbon loss. However, our knowledge is far from sufficient to draw conclusions about the carbon budget in the permafrost regions.

The total area of permafrost regions, including continuous, discontinuous, sporadic, and isolated permafrost zones, is about 21 million km^2 in the Northern Hemisphere, and the actual area underlain by permafrost is about 14 million km^2 (Obu et al., 2019). Therefore, the carbon budget across the entire northern permafrost regions should be examined as an integrated system. Most previous studies modeled the carbon loss from thawing permafrost, while the effects of soil temperature increase on the carbon loss in non-permafrost regions are poorly estimated (Virkkala et al., 2021). Furthermore, the effects of plant growth on the carbon budget in permafrost regions are still controversially debated. There are declarative viewpoints that the permafrost carbon loss cannot be compensated for by increased plant growth in the growing season (Abbott et al., 2016; Schuur et al., 2015), while the results from an ensemble of general circulation models indicate that the positive feedback of permafrost carbon to the global climate will be small due to the increasing of vegetation carbon under a warming climate (Schaphoff et al., 2013).

The terrestrial ecosystem generally uptakes carbon in the growing season and releases carbon in the nongrowing season (López-Blanco et al., 2019; McGuire et al., 2012). The net ecosystem exchange (NEE) represents the balance between CO_2 uptake by photosynthesis and CO_2 release by autotropic respiration and organic matter decomposition. There are great uncertainties in the NEE estimations using process and inversion models (Chaudhary et al., 2020; Keenan & Williams, 2018) due to the differences in the model structure, as well as disagreements on the timing and amount of permafrost carbon release and vegetation (McGuire et al., 2018). For example, based on the analysis of observations, process-based models, and inversion models, it was estimated that the carbon budget in the Arctic tundra ranged from −291 to 80 Tg C y^{-1} (McGuire et al., 2012). Field monitoring across high-latitude regions can provide detailed information about NEE at the site level, but these measurements have rarely extended beyond a decade (Belshe et al., 2013; Li et al., 2021; Schädel et al., 2018). Recently, machine learning and regression models have been used for predicting carbon fluxes based on the relationship between CO_2 flux and predicting variables at the regional scale (Natali et al., 2019, 2022; Warner et al., 2019). Using the machine learning model, the carbon loss during the nongrowing season was estimated at 1,662 Tg per year (Natali et al., 2019). Nevertheless, due to a lack of comprehensive analysis of the carbon exchange in both nongrowing and growing seasons, the annual carbon budget over the high-latitude permafrost regions remains unknown. This knowledge gap represents a major hurdle to the improvement of carbon budget prediction in the permafrost regions and the corresponding economic impacts on the future (Natali et al., 2021; Schuur et al., 2015; Virkkala et al., 2021).

Here, we examine the patterns, processes and driving factors of CO_2 budgets in the growing and nongrowing season. We also estimate the carbon fluxes by 2100 using meteorological data and carbon cycle drivers from ensembles of the Coupled Model Intercomparison Project (CMIP6) for shared socioeconomic pathways (SSPs) 1–2.6, 2–4.5, and 5–8.5. Furthermore, we calculate the economic implications of the carbon budget under different SSPs using the PAGE-ICE model. The workflow is shown in Figure S1 in Supporting Information S1. These efforts provide a temporally and spatially explicit carbon budget pattern and reveal important insights into future permafrost carbon–climate feedbacks and their economic implications in northern high-latitude regions in the future.

2. Data and Methods

2.1. Data Collection

We complied a dataset of in situ CO_2 emissions and potential driving variables, including climatic and environmental variables, during 2002–2017. We used a random forest (RF) machine learning approach to upscale these data to seasonal and annual average NEEs. We defined the nongrowing season from October to April (Natali et al., 2019; Schädel et al., 2018), and the growing season from May to September (Natali et al., 2014). The synthesized dataset includes sites in high-latitude permafrost regions from the literature (Natali et al., 2019) and the global carbon flux network including AmeriFlux (Novick et al., 2018), Asia Flux (Kim et al., 2016) and EuropeFlux database cluster (Paris et al., 2012; Valentini, 2003) (Figure 1, Table S1 in Supporting Information S1). In total, there are 135 sites that measured carbon fluxes in the nongrowing season (October to April) and 55 sites that measured carbon fluxes in the growing season (May to September) (Table S2 in Supporting Information S1). The dataset represents a total of 143 monitoring sites and comprises 608 aggregated monthly fluxes.

The climatic and environmental variables (Table S3 in Supporting Information S1), including air temperature (Ta), soil temperature (Ts), precipitation (P), and leaf area index (LAI), were obtained from the NASA
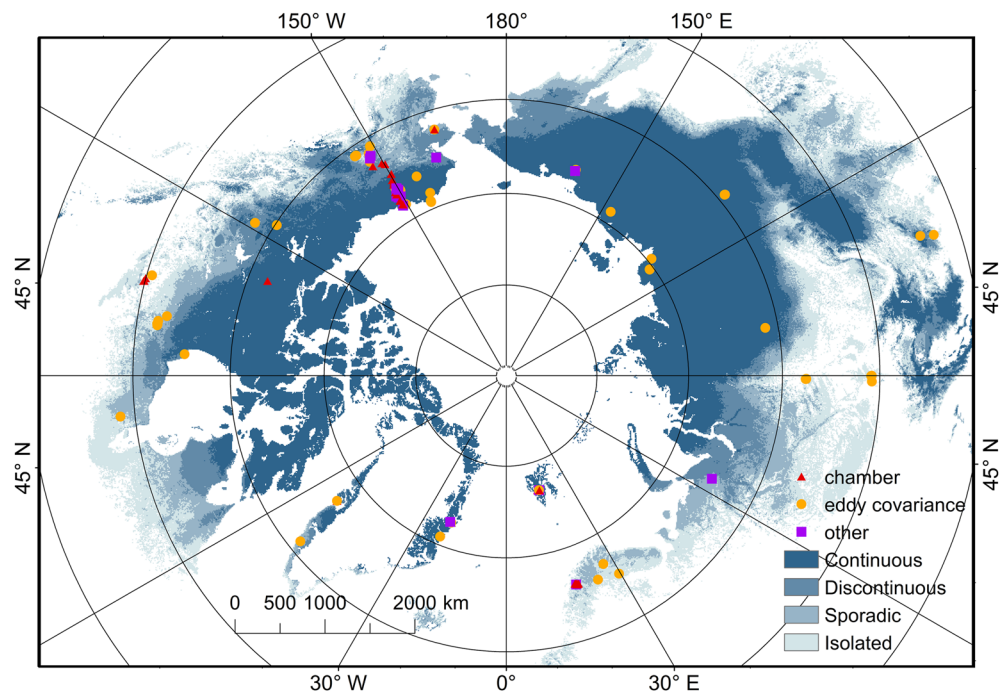
Figure 1. Field stations for CO_2 flux eddy covariance in the northern permafrost regions. There are 42 chamber sites indicated by red triangles (Natali et al., 2019), 80 eddy covariance sites indicated by yellow circles in the growing season and nongrowing season, and 21 sites measured using chambers placed on snow or based on diffusion from snow are indicated by purple rectangles. The permafrost map was obtained from the literature (Obu et al., 2019).

Modern-Era Retrospective analysis for Research and Applications (MERRA-2) product (Gelaro et al., 2017). Gross primary productivity (GPP) data with a resolution of 0.01–0.05° were obtained from the global GPP dataset (1982–2018), which was used in the research on climate change and carbon cycle (Wang et al., 2021). Soil organic carbon (SOC) contents at a depth of 0–30 cm were obtained from the Northern Circumpolar Soil Carbon Database (NCSCD, 0.1° resolution) (Hugelius et al., 2014). Land cover data were retrieved from the European Space Agency (ESA) Climate Change Initiative V.3 land cover classifications (300 m). Soil texture data, including soil sand (S_d), volumetric soil water (S_{vwc}) and soil clay (S_y), were obtained from the Global Soil Dataset for use in Earth System Models (GSDE). All geospatial data were regirded at a resolution of 0.1° prior to CO_2 flux upscaling.

2.2. Data Filtering and Gap Filling

The nongrowing season CO_2 flux data collected using chambers placed on soil, chambers placed on snow, and diffusion from snow were obtained from published literature (Natali et al., 2019). The CO_2 eddy covariance (EC) flux data of nongrowing and growing seasons were downloaded from AmeriFlux, Asia Flux and EuropeFlux. The EC fluxes were calculated for each 30-min interval using the raw data processing software EddyPro (v7.0.6, LI-COR Inc.) (Wutzler et al., 2018). To obtain time series CO_2 flux data, we filled the data gaps using the marginal distribution sampling (MDS) algorithm, implemented in the ReddyProc R package (Wutzler et al., 2018). The missing CO_2 flux values were derived from a look-up table or from the mean diurnal course, depending on the length of the data gap and the availability of meteorological input variables, that is, radiation, air temperature, and water vapor deficit. The look-up table approach replaces the missing value with the average value under similar meteorological conditions within a certain time window (Falge et al., 2001). If the differences in solar radiation, temperature and vapor pressure deficit (VPD) were less than 50 W m^{-2}, 2.5°C, and 5.0 hPa, the meteorological conditions were assumed to be similar, and the blank values were filled using the values under similar meteorological conditions (Nieberding et al., 2020). If there were no similar meteorological conditions within a certain time window, the missing value was replaced using the average value at the same time of the day (1 hr). For some sites that did not meet the criteria for EddyPro processing, we used RF machine learning to fill the gaps (Nemitz

et al., 2018). There were 80 eddy tower sites in this study, of which 23 sites were already processed in the literature (Natali et al., 2019), and 11 sites did not require gap filling. A total of 46 sites need to be interpolated, in which 20 sites were filled up using the look-up table approach of ReddyPro, and the others were processed using RF. The time span of each site that needs to be interpolated is different, which depends on the missing data. All the interpolated data are processed into the monthly data of the corresponding site for spatial upscaling. The gap-filled data met the USTAR criteria through the database processing pipeline. To assess the accuracy of the missing data-filling methods, we randomly selected five sites to compare the data-filling methods using RF and Reddypro. The results showed that relative error (RE), the root mean square error (RMSE) and mean squared error (MAE) values from RF were lower than those of Reddypro (Table S4 in Supporting Information S1), indicating that filling the missing data at the sites using RF was appropriate.

2.3. Random Forest

We used an RF machine learning method to fill the missing data for the 20 sites. The RF model can be run on the R platform. For the model training, the "caret" package was selected to optimize the random forest model. Based on the main factors that affect NEE, we selected inputting parameters for RF: air temperature (Ta), Ts is the soil temperature (Ts), precipitation (P), leaf area index (LAI), and gross primary production (GPP). All of these data were monthly average values. We also included the land cover type (Lc), soil sand (S_d), soil clay (S_y), volumetric soil water content (Svwc) and soil organic carbon content (SOC) in the model (Table S3 in Supporting Information S1). We used a 10-fold cross-validation method to evaluate the accuracy, and the accuracy was evaluated by the root mean squared error (RMSE), mean absolute error (MAE), and coefficient of determination (R^2). The results show that the monthly average R^2 value is 0.388, with RMSE and MAE values of 0.267 and 0.218 g C$-CO_2$ m^{-2} d^{-1} (Table S5 in Supporting Information S1). When the training function is used to improve the performance of the RF model, there will be 3^n models, and n is the number of parameters adjusted in the RF. Then, the RF model automatically selects the best model based on the above three parameters and calculates the relative importance of each driving variable to the NEE.

2.4. Spatial Upscaling of CO_2 Fluxes

We scaled the modeled CO_2 flux data using RF methods to the northern permafrost areas (>45°N) with a total land area of 15.86×10^6 km^2 excluding major lakes. For upscaling these CO_2 fluxes during 2002–2017, the environmental data were extracted from the geographic raster dataset as the driving variables. This multilayer raster dataset was created using the "dismo" package. The total NEE of the growing and nongrowing seasons was simply calculated from the monthly NEE of the entire high-latitude terrestrial ecosystem by summing all the cells. The monthly mean daily CO_2 fluxes (g C$–CO_2$ m^{-2} d^{-1}) were generated for each grid at a resolution of 0.1°. The total high-latitude CO_2 budget was calculated according to the monthly fluxes in the terrestrial area for each grid cell by subtracting the water body fractions (ESACCI-LC-L4-Water Body) from each grid cell area. The calculation method is as follows:

$$S_{NEE} = \sum_i^n NEE_i \times S_{cell} \times d$$

where S_{NEE} is the summed NEE in all high-latitude permafrost regions, NEE_i is the monthly mean estimated value of each grid pixel (g C-CO_2 m^{-2} d^{-1}), i and n are the ordinal and number of pixels, S_{cell} is the area of each grid cell, and d is the day number. To access the uncertainty of the upscaled result, the average root mean square error (RMSE) values outputted by the final model and then the summed RMSE of the entire region were calculated based on the assumption that all the grids had the same RMSE values.

2.5. Comparison of RF With Terrestrial Biosphere Models and Projection of CO_2 Budget

We compared our results in the nongrowing and growing seasons to outputs from 15 Terrestrial Biosphere Models in the Multiscale Synthesis and Terrestrial Model Intercomparison Project (MsTMIP) in the North American Carbon Project (NACP), including the BIOME-BioGeochemical Cycles Model (BIOME-BGC), Community Land Model (CLM), CLM4VIC, the Canadian Land Surface Scheme and Canadian Terrestrial Ecosystem Model (CLASS-CTEM), the Dynamic Land Ecosystem Model (DLEM), the Global Terrestrial Ecosystem Carbon Model (GTEC), the Integrated Science Assessment Model (ISAM), Lund–Potsdam–Jena model (LPJ),

the Organizing Carbon and Hydrology In Dynamic Ecosystems Land Surface Model (ORCHIDEE), the Simple Biosphere Model (Version 3) (SIB3), the combined Simple Biosphere/Carnegie-Ames-Stanford Approach Model (SIBCASA), the Terrestrial Ecosystem Model (Version 6.0) (TEM6), TRIPLEX-GHG, the Vegetation-Global Atmosphere-Soil Model (VEGAS), and the Vegetation Integrative Simulator for Trace gases Model (VISIT) (Jeong et al., 2018). For the projected CO_2 flux, inputs for the RF model of future scenarios of CO_2 budget in nongrowing and growing seasons were obtained from ensembles of Earth System Models (ESM) outputs from the Sixth Coupled Model Intercomparison Project (CMIP6) for SSP1-2.6, SSP2-4.5, and SSP5-8.5. The input variables included the mean monthly winter near-surface air temperature (Ta) and soil temperature (Ts) at 30 cm depth (October-April), annual GPP, mean summer LAI (July and August), and mean monthly summer precipitation (June-August). These data were generated by ensemble r1i1p1f1, derived from 9 models under SSP1-2.6, SSP2-4.5, and SSP5-8.5 (Table S6 and Figure S2 in Supporting Information S1). Ensemble mean SSP1-2.6, SSP2-4.5, and SSP5-8.5 predictor fields were re-projected to the Equal Area Scalable Earth (EASE) 2.0 format of 25 km grids. The output data are the monthly mean NEE (g m^{-2} d^{-1}). The uncertainty of the projected NEE was calculated using a bootstrap method with 1,000 replications, and the 95% confidence interval was generated by the bootstrap method using the "boot" package in R language. The projected NEE from CMIP6 was obtained from the website https://esgf.nci.org.au/search/cmip6-nci/. We searched the data by "nep" as the keyword, which is also called as Net Carbon Mass Flux out of Atmosphere due to Net Ecosystem Productivity (NEP) on Land on the website of CMIP6. We treat the absolute values of NEP and NEE as equivalent (NEE = −NEP). Finally, we selected the NEE data of the models and used the average value as the projected NEE from CMIP6.

2.6. PAGE-ICE Integrated Assessment Model

The latest version of the PAGE-ICE (Aldy et al., 2016; Hope & Schaefer, 2016) model is widely used to assess the potential socio-economic impact that would result from carbon losses from the Arctic permafrost (Chen et al., 2019; Hope & Schaefer, 2016). PAGE-ICE consists of four main modules: emission, climate, discount, and impact. We utilized NEE predictions based on the CMIP6 model and anthropogenic emissions from the Shared Socioeconomic Pathways Database (Riahi et al., 2017) as inputs for the PAGE-ICE emission module to simulate the impact of permafrost carbon sinks on atmospheric greenhouse gas concentrations under future scenarios. Hence, the estimation is primarily influenced by the cross-model uncertainty of NEE simulations. Over time, the estimated impacts of climate change on society are based on an "impact function" that relates gross domestic production losses to global and regional average temperature changes and sea-level changes. PAGE-ICE divides the economic impacts of climate change into four categories, including direct and indirect damages to the overall economy, damages to non-economic sectors such as ecosystem services and public health, the effects of sea-level rise, and large-scale damages associated with tipping points. Based on simulations of future economic and demographic data, the economic impact of NEE changes in permafrost regions is estimated after taking into account the development of climate change adaptation technologies and the cost of emission reductions. The discounting module, taking into account the utility rate of interest and pure time preference rate, compressed future climate damages into a net present value. The parameters of PAGE-ICE adhere to the recommended settings(Yumashev et al., 2019), ensuring consistency and reliability in assessing uncertainty. All results were simulated and run 100,000 times to perturb various model parameters and fully explore the economic impacts.

3. Results

3.1. Effects of Temperature and Other Driving Variables on NEE

Based on the RF model, the relative importance of each driving variable to NEE is shown (Figure 2). Air temperature and precipitation had the most important influence on NEE in the nongrowing season, while leaf area index (LAI) had the most important influence on NEE in the growing season. The air temperature (relative influence 14.6%) and precipitation (14.4%) played much more important roles in the NEE in the nongrowing season. While LAI (13.8%) and air temperature (13.3%) also influenced the CO_2 emissions in the growing season. Air temperature and LAI had the strongest influence on the fluxes with a combined relative influence of 27.0% and 27.8% in the growing and nongrowing seasons, respectively (Figure 2).

Soil temperature significantly influences the NEE in the high-latitude permafrost regions (Figure S3 in Supporting Information S1). During the nongrowing season, CO_2 emissions showed small changes, ranging from 0 to
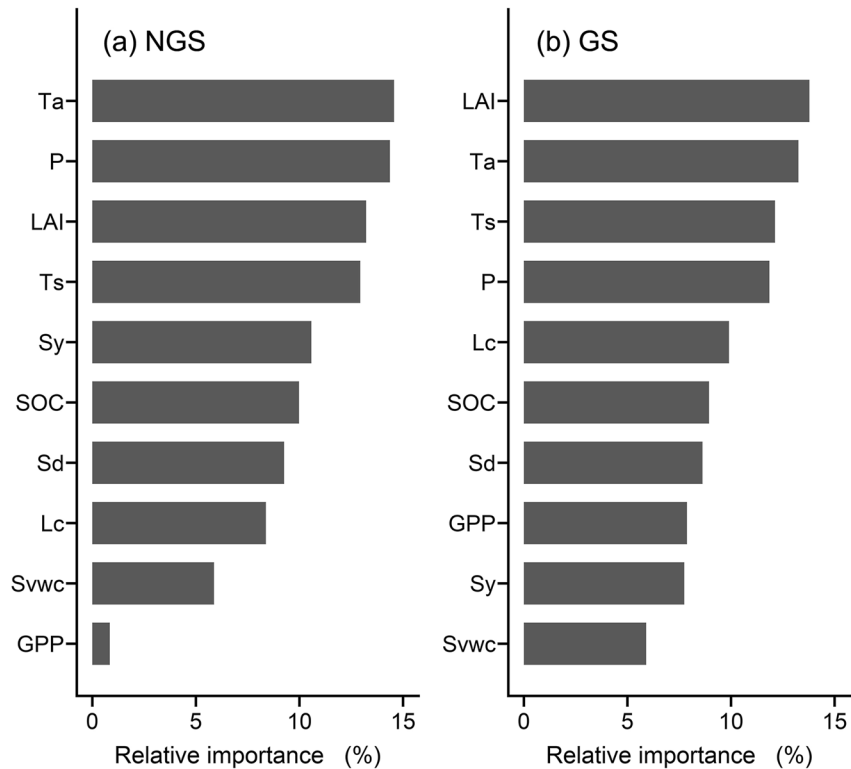
Figure 2. The relative importance of each driving variable to NEE through RF during the non-growing seasons (NGS) (a) and growing seasons (GS) (b). Ta is air temperature, P is precipitation, LAI is leaf area index, Ts is soil temperature, Sy and Sd are soil clay and sand contents, SOC represents soil organic carbon contents, Lc represents land cover types, Svwc is volumetric soil water content, and GPP is gross primary production.

1 g C−CO$_2$ m^{-2} d^{-1} when the soil temperature was below −5°C. When the soil temperature increased from −5°C to 5°C, CO$_2$ emissions increased rapidly. During the growing season, CO$_2$ uptake increased with soil temperature. The CO$_2$ uptake varied from 0 to 1 g C−CO$_2$ m^{-2} d^{-1} when the soil temperature was lower than 5°C. The CO$_2$ uptake increased slightly when the soil temperature was from 5°C to 10°C and increased rapidly when the soil temperature exceeded 10°C. The temperature sensitivity of NEE (Q_{10}) was 9.97 in the nongrowing season and 1.82 in the growing season, respectively (Figure S3 in Supporting Information S1).

3.2. CO$_2$ Flux During the Growing and Nongrowing Seasons

The NEE in the high-latitude permafrost regions has a high spatial heterogeneity (Figure 3, Table S7 in Supporting Information S1). The total annual CO$_2$ uptake is 2,330 Tg C−CO$_2$, with an uncertainty of 960 Tg C−CO$_2$ during the growing season. The CO$_2$ uptake is relatively low at latitudes of 65°–75°N with an NEE of −95 to −65 g C−CO$_2$ m^{-2} yr^{-1}, with the highest uptake values in the low latitudes of Northern America and Siberia. CO$_2$ uptake during the growing season largely decreases with latitude (Figure 3a). During the nongrowing season, the total annual CO$_2$ emissions are 1,539 Tg C−CO$_2$, with a corresponding flux uncertainty of 392 Tg C−CO$_2$ during the nongrowing season. The CO$_2$ emissions largely decrease with latitude, with the NEE in the nongrowing season ranging from 20 to 69 g C−CO$_2$ m^{-2} yr^{-1} at latitudes of 60°N–75°N and 55–85 g C−CO$_2$ m^{-2} yr^{-1} at the latitudes of 45°–60°N (Figure 3b). Furthermore, the spatial uncertainties of NEE are shown in Figure S4 in Supporting Information S1.

3.3. Projected CO$_2$ Flux Under Future Climate Warming

We calculate the future growing and nongrowing season CO$_2$ exchanges using the RF model with environmental factors from the sixth Coupled Model Intercomparison Project (CMIP6) earth system model. Both the CO$_2$ uptake during the growing season and CO$_2$ emissions during the nongrowing season significantly increase under
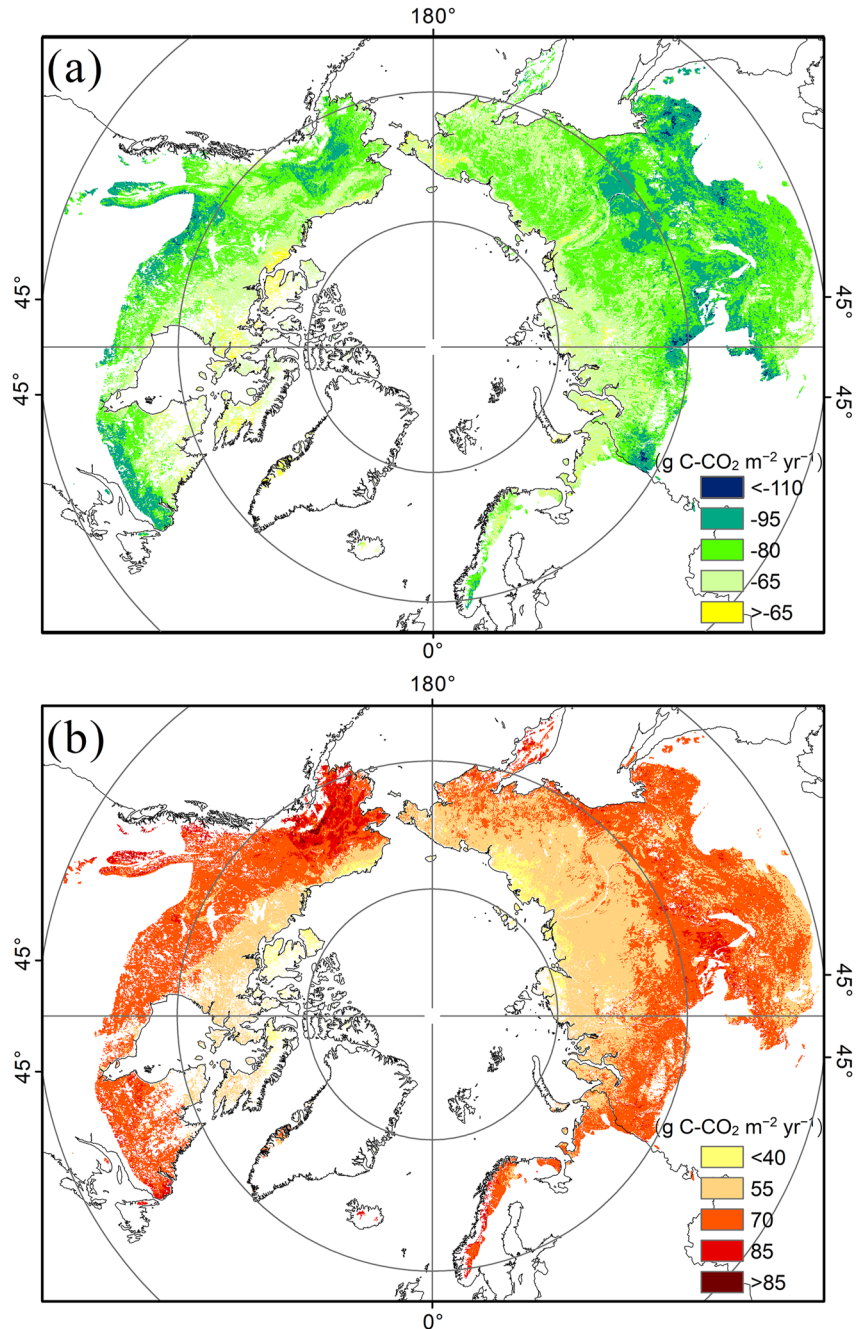
Figure 3. The spatial distribution of NEE during the growing season (a) and nongrowing season (b) in the northern permafrost regions for the baseline years 2002–2017.

the three emission pathway scenarios (Figure S5 in Supporting Information S1). The annual average estimate calculated by the RF in the nongrowing season was lower than the average estimates of 1,950 ± 1,019 Tg C per year for the same study area from the models in MsTMIP (Figures S6 and S7 in Supporting Information S1). Compared with the carbon budget during 2002–2017, both the CO_2 uptake during the growing season and CO_2 emissions during the non-growing season increase under different emission pathways (Figure 4).

From 2018 to 2100, we estimated cumulative CO_2 emissions of 180 Pg C, 196 Pg C, and 242 Pg C during the nongrowing season for SSP1-2.6, SSP2-4.5, and SSP5-8.5 (Figure S8a in Supporting Information S1). While during the growing season, the cumulative CO_2 uptake was 234 Pg C, 235 Pg C, and 243 Pg C for SSP1-2.6,

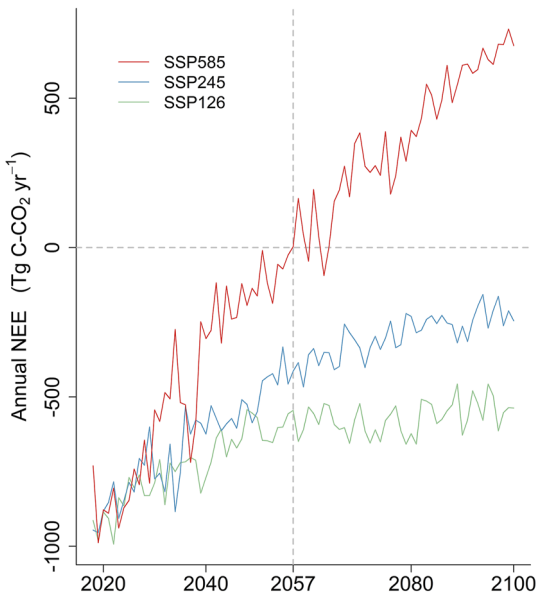**Figure 4.** Projected annual NEE of CO_2 using a random forest model under the shared socioeconomic pathways (SSPs) 1–2.6, 2–4.5, and 5–8.5.

SSP2-4.5, and SSP5-8.5 (Figure S8b in Supporting Information S1). Based on the RF model, the annual NEE represents a carbon sink with a weakening trend under all the SSPs, indicating that climate warming will reduce the carbon sink of the northern permafrost regions. For the SSP5-8.5, the NEE represented a carbon source after 2057. The total CO_2 uptake is approximately 18 Pg C during 2020–2056, and carbon release is approximately 17 Pg C during 2057–2100 (Figure 4).

3.4. Economic Implications of Carbon Budget

Under the SSP1-2.6 and SSP2-4.5 pathways, the net ecosystem benefits show a slowing increase due to the gradual decline in the carbon sink. This suggests that the capacity of ecosystems to sequester carbon may diminish over time under these scenarios. However, the economic benefits remain similar upward trends because the changes in NEE and global gross domestic production (GDP) are similar under the two pathways. This implies that the economic gains from other factors offset the decreasing carbon sink. In contrast, the SSP5-8.5 pathway portrays a concerning trend in ecosystem benefits. Around 2070, these benefits start to decline, indicating a potential deterioration of ecosystem services due to the exacerbation of climate change. The economic consequences are also notable, as the mean economic benefit decreases from $87.5 billion/yr in 2070 to $58.9 billion/yr in 2100. This suggests that the economic losses resulting from becoming a carbon source outweigh the growth of GDP. Such a situation implies the need for stringent measures to mitigate greenhouse gas emissions and limit the adverse economic impacts associated with high-emission pathways. To assess the long-term economic implications, we incorporated the concepts of time value of money and discounting to provide an estimate of the total net economic benefits over the period 2021–2100. The results indicate that the SSP1-2.6 pathway is projected to yield total net economic benefits of $4.5 (5%–95% range: $2.6–$10.5) trillion. Similarly, the values for the SSP2-4.5 and SSP5-8.5 pathways are projected to be $5.0 (5%–95% range: $1.9–9.2) trillion and $2.9 (5%–95% range: $1.0–4.3) trillion, respectively (Figure 5).

4. Discussion

Our framework is unique in that it compiles a new dataset of growing and nongrowing seasons using chamber data and eddy covariance and investigates their respective drivers of these fluxes. CO_2 emissions in the nongrowing season increased by a factor of 9.97 per 10°C soil temperature increase (Q_{10}) and by a factor of 1.82 for CO_2 uptake in the growing season. The differences in Q_{10} both in the nongrowing and growing seasons show that
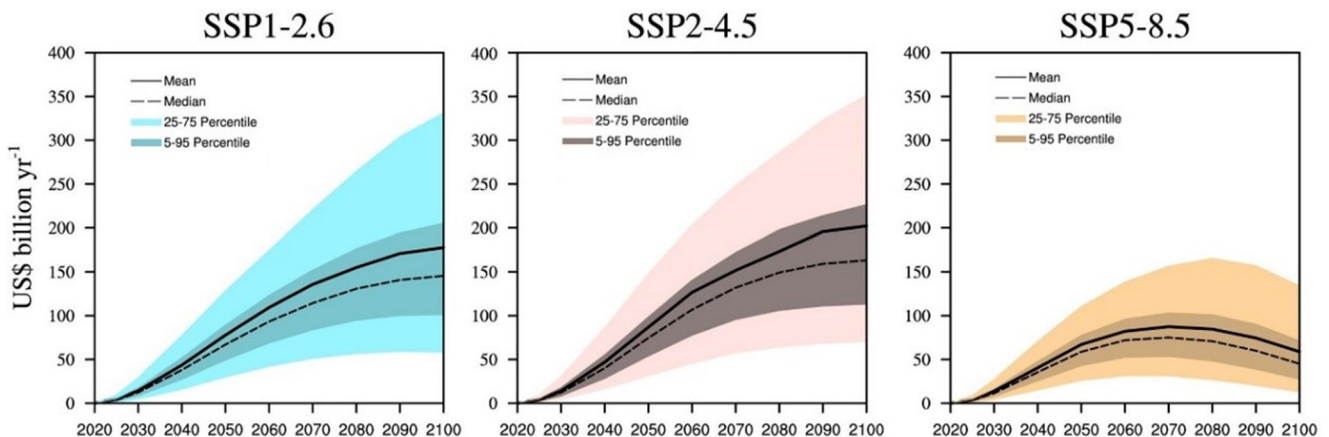

Figure 5. Predicted annual economic impact due to the NEE under SSP1-2.6, SSP2-4.5 and SSP5-8.5.

CO_2 exchange is more sensitive to the nongrowing season warming. Thus, it further confirms that enhanced soil carbon loss due to winter warming may offset growing season CO_2 uptake under future climate warming (Natali et al., 2019). CO_2 emissions are relatively low below −5°C because cold temperature and low unfrozen water content limit microbial decomposition (Mu et al., 2016). When the temperature increases from −5°C to 5°C during the nongrowing season, there is a drastic increase in CO_2 emissions. It has been demonstrated that when the soil temperature is around the freezing point, organic matter decomposition is mainly controlled by temperature (Mikan et al., 2002; Mu et al., 2016). During the growing season, the NEE shows small changes when the temperature increases from −5°C to 5°C. This can be explained by the fact that increasing temperature can accelerate soil organic matter decomposition, while the plants are also able to recover and uptake carbon (Schädel et al., 2018). When the soil temperature is above 10°C, the CO_2 uptake increases with temperature, suggesting that CO_2 emissions are overwhelmed by vegetation growth during the growing season (Emmerton et al., 2016; Forkel et al., 2016; Mu et al., 2017). Thus, the negative relationship between NEE and temperature could be explained by the fact that high temperature can promote vegetation growth, thereby improving the photosynthesis and carbon uptake (Yao et al., 2022).

Air temperature is the most important driver of NEE, followed by leaf area index and precipitation. In the non-growing season, soil temperature controls soil respiration (Natali et al., 2019). In the growing season, soil temperature, air temperature, and leaf area index are closely associated with plant growth (Walker et al., 2003). GPP plays a less important role in NEE during the nongrowing season because the NEE is dominated by soil respiration in the CO_2 uptake period (Watts et al., 2021). Another possible explanation is that GPP across large scales is dependent on the temperature in the growing season, length of season, and radiation, which regulate and provide resources for plant growth (López-Blanco et al., 2017; Virkkala et al., 2021). In general, we found that warmer and wetter conditions and better vegetation with high LAI and GPP increased the magnitude of annual NEE. The CO_2 budget in the growing and nongrowing seasons is latitude dependent within the northern permafrost domain (>45°N), with higher carbon uptake and carbon emission in the low-latitude permafrost areas. This is in agreement with the decreased trends of annual NEE with increasing latitude for both deciduous broadleaf forests and evergreen needleleaf forests (Yuan et al., 2009). This is because air temperature was the primary influencing factor.

The CO_2 emission in our result (1,539 ± 392 Tg C per year) in the nongrowing season (October to April) was similar to the previous study (1,662 ± 813 Tg C per year) based on boosted regression tree analysis (Natali et al., 2019). Our study involved more field site data than previous reports, and more efforts in the future should be made to measure fluxes over the entire year in as many sites as possible in order to obtain better upscaling results. Although the uncertainties introduced by gap-filling remain, the variation in annual CO_2 emissions between multiple methods was small(Desai et al., 2008). Since this study is not designed for the explorations of how the different gap-filling approaches influence fluxes, understanding the uncertainties caused by gap-filling remains an important research priority (Virkkala et al., 2021). The differences between the RF and models in MsTMIP (Figures S6 and S7 in Supporting Information S1) can be attributed to the different upscaling methods and the number of monitoring sites. To decrease the differences between our simulation and the Terrestrial Biosphere Models, some areas with few monitoring sites such as central Siberia, European Russia, Canada and Mongolia should pay more attention to understanding the sink-source patterns of permafrost regions.

During the growing season (May to September) in 2002–2017, our results have a similar pattern with the estimates from the models in MsTMIP (Figure S7 in Supporting Information S1). We estimated approximately −2,330 Tg C per year with a flux uncertainty of 960 Tg C per year, which is much higher than that derived from process-based terrestrial models (−687 to −1,647 Tg C) (Natali et al., 2019). The carbon assimilation during the growing season in our study is comparable with the results (−1,261 to −3,566 Tg C per year) from the MsTMIP models (Figure S7 in Supporting Information S1). These differences can be attributed to the different parameterization schemes and structures in the models, and different environmental gradients (Pastorello et al., 2020). Predictions based on machine learning methods have been shown to have higher model accuracy and transferability (Tramontana et al., 2016). Furthermore, it performed well when predicting to the same data that the models were trained with (Virkkala et al., 2021). Therefore, our results were comparable to those of the Terrestrial Biosphere Models in the non-growing seasons and growing seasons. Compared to the nongrowing season, higher uncertainties and lower predictive performance existed in the growing season because the variable growing season measurement periods were used in the NEE across the studies (Virkkala et al., 2021). Therefore, it is urgent to build models at a finer temporal resolution, especially in the growing season, so that we can better

estimate the NEE and capture rapidly changing transition periods. There are greater heterogeneities in the spatial distribution of NEE, which can be attributed to the comprehensive effects of influential factors, including the soil temperature and water content, soil carbon content, vegetation and snow cover (Forkel et al., 2016; Jafarov & Schaefer, 2016; Loranty et al., 2018). Both the CO_2 emissions in the non-growing season and CO_2 uptake in the growing season changed with latitude, with higher values in forests and grasslands at lower latitudes (Xue et al., 2021).

The projected annual NEE in our study shows that the terrestrial ecosystem will shift to a carbon source after 2057 under the SSP5-8.5. In a previous report, the results from several models suggested that the substantial net losses of ecosystem carbon would not occur until after 2100 (McGuire et al., 2018). The projected carbon emissions in the nongrowing season are similar to projections from the CMIP6 ESM ensemble (Figure S8 in Supporting Information S1), which suggests that our data-driven RF model may offer good NEE estimates in the nongrowing season. The projected CO_2 uptake during the growing season is substantially lower than the values from ESMs in CMIP6 (Figure S8 in Supporting Information S1). Since the increasing trends of the effects of climate warming and CO_2 fertilization on vegetation photosynthesis will slow (Piao et al., 2017; Wang et al., 2020), the CO_2 uptake in the growing season may decrease. The RF model may provide more conservative estimates because current in situ observations may not adequately reflect future environmental responses to substantially warming growing seasons. However, the present ESMs are possibly missing the permafrost thawing processes and mechanisms that might lead to current uncertainties in the estimates of growing and nongrowing CO_2 exchange (Natali et al., 2019; Turetsky et al., 2020). Although there are still great uncertainties in future prediction, we highlight the importance of the responses of NEE in nongrowing and growing seasons to warming in the future ESMs when predicting permafrost carbon dynamics in a changing environment.

The net economic benefit will be reduced by about 50% under SSP5-8.5 in comparison with SSP1-2.6 pathways. Under the SSP1-2.6 and SSP2-4.5 pathways, the slowing increase trends of the net ecosystem benefits are similar to the gradually decreasing CO_2 uptake rates. For the SSP5-8.5 pathway, the CO_2 uptake during 2020–2056 (18 Pg) is similar to the CO_2 emissions during 2057–2100 (17 Pg). As a result, although the northern permafrost regions shift to a carbon source since 2057, the overall economic effects are still positive. These results are different from the previous results that the permafrost carbon emissions in the northern permafrost will cause serious economic loss (Chen et al., 2019; Hope & Schaefer, 2016). The main reason for this difference is that previous studies focused on the economic impacts of the carbon loss from permafrost-affected soils (Chen et al., 2019; Hope & Schaefer, 2016), while our study considered the NEE from the permafrost regions. Our findings underscore the importance of considering both ecological and economic factors when formulating climate change mitigation and adaptation strategies. The analysis reveals that pursuing low-emission pathways (SSP1-2.6) can potentially lead to higher net economic benefits, whereas high-emission pathways (SSP5-8.5) may result in economic losses due to carbon emissions and NEE changes in permafrost regions. Policymakers and stakeholders should take these projected economic impacts into account and prioritize actions that align with sustainable development goals, balancing environmental protection and economic growth.

There are great uncertainties in the carbon cycle in the northern permafrost regions among different terrestrial biosphere models (Fisher et al., 2014; McGuire et al., 2018). Our results show that the annual NEE will change from a CO_2 uptake to a release in the 2060s under the SSP5-8.5, while we stress that the northern permafrost regions will be likely to act as carbon sources much earlier than that. This is because the NEE value is much lower than the net biome productivity (NBP), which represents a long-term carbon storage. Globally, disturbance or harvest accounts for a very important part of the NEE (Schuur et al., 2022; Wilkinson et al., 2023). It has been reported that the soil carbon pool during 2000–2009 is almost static in the northern permafrost regions (Abbott et al., 2016). Therefore, although the negative NEE in our results indicates carbon assimilation by plants, some of the carbon may be released back into the air through other mechanisms (Raymond et al., 2013; Schuur et al., 2022; Wik et al., 2016; Wilkinson et al., 2023). For example, wildfires led to a carbon loss of approximately 260 Tg C per year in the 2010s (Abbott et al., 2016), riverine-exported carbon reached 40 Tg C per year (Karlsson et al., 2021; Mu et al., 2019; Serikova et al., 2018), and CO_2 emissions from rivers were much higher than the exported values (Raymond et al., 2013). In addition, CO_2 emissions from lakes (Elder et al., 2018; Wik et al., 2016), thermokarst landscapes (Turetsky et al., 2020) and coastal erosion (Nielsen et al., 2022) are not negligible. Abrupt thaw and wildfire disturbance are not simulated in any Earth System Model, which results in large uncertainties in future Arctic permafrost carbon budgets due to climate change (Miner et al., 2022; Turetsky et al., 2020). Furthermore, permafrost regions have a great potential to emit much more CH_4 (Treat et al., 2018; Zona et al., 2016). It was

estimated that regional CH_4 emissions from tundra and boreal wetlands were approximately 35 Tg CH_4-C year^{-1} using a satellite data-driven process-model for northern ecosystems (Watts et al., 2023). Similar to CO_2 emissions, understanding CH_4 emission magnitude and its driving factors in the growing and nongrowing seasons still requires more in situ observations to narrow the uncertainties of the carbon budget.

5. Conclusions

Our results showed that the current carbon release is 1,539 Tg C (with an uncertainty of 392 Tg C) per year in the northern permafrost regions during the non-growing seasons (October-April) and uptake is 2,330 Tg C (with an uncertainty of 960 Tg C) per year during the growing seasons (May-September). The terrestrial ecosystem would be a carbon sink by 2100 under SSP1-2.6 and SSP2-4.5, but it will shift to a carbon source after 2057 under SSP5-8.5. Since there are other disturbances such as wild fire and development of thermokarst terrains can release carbon, there is a high risk that permafrost ecosystems will shift from carbon sinks to sources in the future. Without considering other processes of carbon loss, the cumulative economic impacts of the carbon budget changes during 2020–2100 are largely positive, while the economic benefits under SSP5-8.5 will be only half that of SSP1-2.6. Our results provide a deep insight into understanding how much carbon has been assimilated and released in northern permafrost ecosystems. Our findings have important implications for the future role of northern permafrost in regulating the ecosystem carbon cycle and economic benefit.

Data Availability Statement

All the data and the code are available at Zenodo via https://zenodo.org/record/8185908 (Mu et al., 2023).

References

Abbott, B. W., Jones, J. B., Schuur, E. A. G., Chapin III, F. S., Bowden, W. B., Bret-Harte, M. S., et al. (2016). Biomass offsets little or none of permafrost carbon release from soils, streams, and wildfire: An expert assessment. *Environmental Research Letters*, *11*(3), 034014. https://doi.org/10.1088/1748-9326/11/3/034014

Aldy, J., Pizer, W., Tavoni, M., Reis, L. A., Akimoto, K., Blanford, G., et al. (2016). Economic tools to promote transparency and comparability in the Paris Agreement. *Nature Climate Change*, *6*(11), 1000–1004. https://doi.org/10.1038/nclimate3106

Belshe, E., Schuur, E., & Bolker, B. (2013). Tundra ecosystems observed to be CO_2 sources due to differential amplification of the carbon cycle. *Ecology Letters*, *16*(10), 1307–1315. https://doi.org/10.1111/ele.12164

Burke, E. J., Jones, C. D., & Koven, C. D. (2013). Estimating the Permafrost-Carbon climate response in the CMIP5 climate models using a simplified approach. *Journal of Climate*, *26*(14), 4897–4909. https://doi.org/10.1175/JCLI-D-12-00550.1

Chaudhary, N., Westermann, S., Lamba, S., Shurpali, N., Sannel, A. B. K., Schurgers, G., et al. (2020). Modelling past and future peatland carbon dynamics across the pan-Arctic. *Global Change Biology*, *26*(7), 4119–4133. https://doi.org/10.1111/gcb.15099

Chen, Y., Liu, A., Zhang, Z., Hope, C., & Crabbe, M. J. C. (2019). Economic losses of carbon emissions from circum-Arctic permafrost regions under RCP-SSP scenarios. *Science of the Total Environment*, *658*, 1064–1068. https://doi.org/10.1016/j.scitotenv.2018.12.299

Deimling, T. S. V., Meinshausen, M., Levermann, A., Huber, V., Frieler, K., Lawrence, D. M., & Brovkin, V. (2012). Estimating the near-surface permafrost-carbon feedback on global warming. *Biogeosciences*, *9*(2), 649–665. https://doi.org/10.5194/bg-9-649-2012

Desai, A. R., Richardson, A. D., Moffat, A. M., Kattge, J., Hollinger, D. Y., Barr, A., et al. (2008). Cross-site evaluation of eddy covariance GPP and RE decomposition techniques. *Agricultural and Forest Meteorology*, *148*(6–7), 821–838. https://doi.org/10.1016/j.agrformet.2007.11.012

Elder, C. D., Xu, X., Walker, J., Schnell, J. L., Hinkel, K. M., Townsend-Small, A., et al. (2018). Greenhouse gas emissions from diverse Arctic Alaskan lakes are dominated by young carbon. *Nature Climate Change*, *8*(2), 166–171. https://doi.org/10.1038/s41558-017-0066-9

Emmerton, C. A., Louis, V. L. S., Humphreys, E. R., Gamon, J. A., Barker, J. D., & Pastorello, G. Z. (2016). Net ecosystem exchange of CO_2 with rapidly changing high Arctic landscapes. *Global Change Biology*, *22*(3), 1185–1200. https://doi.org/10.1111/gcb.13064

Falge, E., Baldocchi, D., Olson, R., Anthoni, P., Aubinet, M., Bernhofer, C., et al. (2001). Gap filling strategies for long term energy flux data sets. *Agricultural and Forest Meteorology*, *107*(1), 71–77. https://doi.org/10.5194/bgd-10-17785-2013

Fisher, J. B., Sikka, M., Oechel, W. C., Huntzinger, D. N., Melton, J. R., Koven, C. D., et al. (2014). Carbon cycle uncertainty in the Alaskan Arctic. *Biogeosciences*, *11*(15), 4271–4288. https://doi.org/10.5194/bg-11-4271-2014

Forkel, M., Carvalhais, N., Rödenbeck, C., Keeling, R., Heimann, M., Thonicke, K., et al. (2016). Enhanced seasonal CO_2 exchange caused by amplified plant productivity in northern ecosystems. *Science*, *351*(6274), 696–699. https://doi.org/10.1126/science.aac4971

Gelaro, R., McCarty, W., Suárez, M. J., Todling, R., Molod, A., Takacs, L., et al. (2017). The modern-era retrospective analysis for research and applications, version 2 (MERRA-2). *Journal of Climate*, *30*(14), 5419–5454. https://doi.org/10.1175/JCLI-D-16-0758.1

Hope, C., & Schaefer, K. (2016). Economic impacts of carbon dioxide and methane released from thawing permafrost. *Nature Climate Change*, *6*(1), 56–59. https://doi.org/10.1038/nclimate2807

Hugelius, G., Strauss, J., Zubrzycki, S., Harden, J. W., Schuur, E., Ping, C.-L., et al. (2014). Estimated stocks of circumpolar permafrost carbon with quantified uncertainty ranges and identified data gaps. *Biogeosciences*, *11*(23), 6573–6593. https://doi.org/10.5194/bg-11-6573-2014

Jafarov, E., & Schaefer, K. (2016). The importance of a surface organic layer in simulating permafrost thermal and carbon dynamics. *The Cryosphere*, *10*(1), 465–475. https://doi.org/10.5194/tc-10-465-2016

Jeong, S.-J., Bloom, A. A., Schimel, D., Sweeney, C., Parazoo, N. C., Medvigy, D., et al. (2018). Accelerating rates of Arctic carbon cycling revealed by long-term atmospheric CO_2 measurements. *Science Advances*, *4*(7), eaao1167. https://doi.org/10.1126/sciadv.aao1167

Karlsson, J., Serikova, S., Vorobyev, S. N., Rocher-Ros, G., Denfeld, B., & Pokrovsky, O. S. (2021). Carbon emission from Western Siberian inland waters. *Nature Communications*, *12*(1), 825. https://doi.org/10.1038/s41467-021-21054-1

Keenan, T., & Williams, C. (2018). The terrestrial carbon sink. *Annual Review of Environment and Resources*, *43*(1), 219–243. https://doi.org/10.1146/annurev-environ-102017-030204

Kim, D., Lim, Y.-J., Kang, M., & Choi, M. (2016). Land response to atmosphere at different resolutions in the common land model over East Asia. *Advances in Atmospheric Sciences*, *33*(3), 391–408. https://doi.org/10.1007/s00376-015-5059-x

Koven, C. D., Ringeval, B., Friedlingstein, P., Ciais, P., Cadule, P., Khvorostyanov, D., et al. (2011). Permafrost carbon-climate feedbacks accelerate global warming. *Proceedings of the National Academy of Sciences of the United States of America*, *108*(36), 14769–14774. https://doi.org/10.1073/pnas.1103910108

Li, Z.-L., Mu, C. C., Chen, X., Wang, X. Y., Dong, W. W., Jia, L., et al. (2021). Changes in net ecosystem exchange of CO2 in Arctic and their relationships with climate change during 2002–2017. *Advances in Climate Change Research*, *12*(4), 475–481. https://doi.org/10.1016/j.accre.2021.06.004

López-Blanco, E., Exbrayat, J.-F., Lund, M., Christensen, T. R., Tamstorf, M. P., Slevin, D., et al. (2019). Evaluation of terrestrial pan-Arctic carbon cycling using a data-assimilation system. *Earth System Dynamics*, *10*(2), 233–255. https://doi.org/10.5194/esd-10-233-2019

López-Blanco, E., Lund, M., Williams, M., Tamstorf, M. P., Westergaard-Nielsen, A., Exbrayat, J.-F., et al. (2017). Exchange of CO 2 in Arctic tundra: Impacts of meteorological variations and biological disturbance. *Biogeosciences*, *14*(19), 4467–4483. https://doi.org/10.5194/bg-14-4467-2017

Loranty, M. M., Abbott, B. W., Blok, D., Douglas, T. A., Epstein, H. E., Forbes, B. C., et al. (2018). Reviews and syntheses: Changing ecosystem influences on soil thermal regimes in northern high-latitude permafrost regions. *Biogeosciences*, *15*(17), 5287–5313. https://doi.org/10.5194/bg-15-5287-2018

Masson-Delmotte, V., Zhai, P., Pirani, A., Connors, S. L., Péan, C., Berger, S., et al. (2021). *Climate change 2021: The physical science basis. Contribution of working group I to the sixth assessment report of the Intergovernmental Panel on Climate Change*. IPCC. https://doi.org/10.1017/9781009157896

McGuire, A., Christensen, T., Hayes, D., Heroult, A., Euskirchen, E., Kimball, J., et al. (2012). An assessment of the carbon balance of Arctic tundra: Comparisons among observations, process models, and atmospheric inversions. *Biogeosciences*, *9*(8), 3185–3204. https://doi.org/10.5194/bg-9-3185-2012

McGuire, A. D., Lawrence, D. M., Koven, C., Clein, J. S., Burke, E., Chen, G., et al. (2018). Dependence of the evolution of carbon dynamics in the northern permafrost region on the trajectory of climate change. *Proceedings of the National Academy of Sciences of the United States of America*, *115*(15), 3882–3887. https://doi.org/10.1073/pnas.1719903115

Mikan, C. J., Schimel, J. P., & Doyle, A. P. (2002). Temperature controls of microbial respiration in arctic tundra soils above and below freezing. *Soil Biology and Biochemistry*, *34*(11), 1785–1795. https://doi.org/10.1016/S0038-0717(02)00168-2

Miner, K. R., D'Andrilli, J., Mackelprang, R., Edwards, A., Malaska, M. J., Waldrop, M. P., & Miller, C. E. (2021). Emergent biogeochemical risks from Arctic permafrost degradation. *Nature Climate Change*, *11*(10), 809–819. https://doi.org/10.1038/s41558-021-01162-y

Miner, K. R., Turetsky, M. R., Malina, E., Bartsch, A., Tamminen, J., McGuire, A. D., et al. (2022). Permafrost carbon emissions in a changing Arctic. *Nature Reviews Earth & Environment*, *3*(1), 55–67. https://doi.org/10.1038/s43017-021-00230-3

Mu, C., Zhang, F., Chen, X., Ge, S., Mu, M., Jia, L., et al. (2019). Carbon and mercury export from the Arctic rivers and response to permafrost degradation. *Water Research*, *161*, 54–60. https://doi.org/10.1016/j.watres.2019.05.082

Mu, C., Zhang, T., Zhang, X. Y., Cao, B., & Peng, X. (2016). Sensitivity of soil organic matter decomposition to temperature at different depths in permafrost regions on the northern Qinghai-Tibet Plateau. *European Journal of Soil Science*, *67*(6), 773–781. https://doi.org/10.1111/ejss.12386

Mu, C., Zhang, T., Zhao, Q., Su, H., Wang, S., Cao, B., et al. (2017). Permafrost affects carbon exchange and its response to experimental warming on the northern Qinghai-Tibetan Plateau. *Agricultural and Forest Meterology*, *247*, 252–259. https://doi.org/10.1016/j.agrformet.2017.08.009

Mu, C., Zhang, W., Zhuang, Q., & Wu, X. (2023). CO2 budget in the northern permafrost regions(Version 2) [Dataset]. Zenodo. https://doi.org/10.5281/zenodo.8185908

Natali, S. M., Holdren, J. P., Rogers, B. M., Treharne, R., Duffy, P. B., Pomerance, R., & MacDonald, E. (2021). Permafrost carbon feedbacks threaten global climate goals. *Proceedings of the National Academy of Sciences of the United States of America*, *118*(21), e2100163118. https://doi.org/10.1073/pnas.2100163118

Natali, S. M., Rogers, B. M., Watts, J. D., Savage, K., Connon, S. J., Mauritz, M., et al. (2022). The ABCflux database: Arctic–boreal CO 2 flux observations and ancillary information aggregated to monthly time steps across terrestrial ecosystems. *Earth System Science Data*, *14*(1), 179–208. https://doi.org/10.5194/essd-14-179-2022

Natali, S. M., Schuur, E. A. G., Webb, E. E., Pries, C. E. H., & Crummer, K. G. (2014). Permafrost degradation stimulates carbon loss from experimentally warmed tundra. *Ecology*, *95*(3), 602–608. https://doi.org/10.1890/13-0602.1

Natali, S. M., Watts, J. D., Rogers, B. M., Potter, S., Ludwig, S. M., Selbmann, A. K., et al. (2019). Large loss of CO_2 in winter observed across the northern permafrost region. *Nature Climate Change*, *9*(11), 852–857. https://doi.org/10.1038/s41558-019-0592-8

Nemitz, E., Mammarella, I., Ibrom, A., Aurela, M., Burba, G. G., Dengel, S., et al. (2018). Standardisation of eddy-covariance flux measurements of methane and nitrous oxide. *International Agrophysics*, *32*(4), 517–549. https://doi.org/10.1515/intag-2017-0042

Nieberding, F., Wille, C., Fratini, G., Asmussen, M. O., Wang, Y., Ma, Y., & Sachs, T. (2020). A long-term (2005–2019) eddy covariance data set of CO_2 and H_2O fluxes from the Tibetan alpine steppe. *Earth System Science Data*, *12*(4), 2705–2724. https://doi.org/10.5194/essd-12-2705-2020

Nielsen, D. M., Pieper, P., Barkhordarian, A., Overduin, P., Ilyina, T., Brovkin, V., et al. (2022). Increase in Arctic coastal erosion and its sensitivity to warming in the twenty-first century. *Nature Climate Change*, *12*(3), 263–270. https://doi.org/10.1038/s41558-022-01281-0

Novick, K. A., Biederman, J., Desai, A., Litvak, M., Moore, D. J., Scott, R., & Torn, M. (2018). The AmeriFlux network: A coalition of the willing. *Agricultural and Forest Meteorology*, *249*, 444–456. https://doi.org/10.1016/j.agrformet.2017.10.009

Obu, J., Westermann, S., Bartsch, A., Berdnikov, N., Christiansen, H. H., Dashtseren, A., et al. (2019). Northern Hemisphere permafrost map based on TTOP modelling for 2000–2016 at 1 km² scale. *Earth-Science Reviews*, *193*, 299–316. https://doi.org/10.1016/j.earscirev.2019.04.023

Paris, J.-D., Ciais, P., Rivier, L., Chevallier, F., Dolman, H., Flaud, J.-M., et al. (2012). Integrated carbon observation system. In *Paper presented at EGU general assembly conference abstracts*.

Pastorello, G., Trotta, C., Canfora, E., Chu, H., Christianson, D., Cheah, Y., et al. (2020). The FLUXNET2015 dataset and the ONEFlux processing pipeline for eddy covariance data. *Scientific Data*, *7*(1), 225. https://doi.org/10.1038/s41597-020-0534-3

Piao, S., Liu, Z., Wang, T., Peng, S., Ciais, P., Huang, M., et al. (2017). Weakening temperature control on the interannual variations of spring carbon uptake across northern lands. *Nature Climate Change*, *7*(5), 359–363. https://doi.org/10.1038/nclimate3277

Raymond, P. A., Hartmann, J., Lauerwald, R., Sobek, S., Mcdonald, C. P., Hoover, M. D., et al. (2013). Global carbon dioxide emissions from inland waters. *Nature*, *503*(7476), 355–359. https://doi.org/10.1038/nature12760

Riahi, K., Van Vuuren, D. P., Kriegler, E., Edmonds, J., O'neill, B. C., Fujimori, S., et al. (2017). The Shared Socioeconomic Pathways and their energy, land use, and greenhouse gas emissions implications: An overview. *Global Environmental Change*, *42*, 153–168. https://doi.org/10.1016/j.gloenvcha.2016.05.009

Schädel, C., Koven, C. D., Lawrence, D. M., Celis, G., Garnello, A. J., Hutchings, J., et al. (2018). Divergent patterns of experimental and model-derived permafrost ecosystem carbon dynamics in response to Arctic warming. *Environmental Research Letters*, *13*(10), 105002. https://doi.org/10.1088/1748-9326/aae0ff

Schaefer, K., Zhang, T., Bruhwiler, L., & Barrett, A. P. (2011). Amount and timing of permafrost carbon release in response to climate warming. *Tellus B: Chemical and Physical Meteorology*, *63*(2), 165–180. https://doi.org/10.1111/j.1600-0889.2011.00527.x

Schaphoff, S., Heyder, U., Ostberg, S., Gerten, D., Heinke, J., & Lucht, W. (2013). Contribution of permafrost soils to the global carbon budget. *Environmental Research Letters*, *8*(1), 014026. https://doi.org/10.1088/1748-9326/8/1/014026

Schuur, E. A., McGuire, A. D., Schädel, C., Grosse, G., Harden, J. W., Hayes, D. J., et al. (2015). Climate change and the permafrost carbon feedback. *Nature*, *520*(7546), 171–179. https://doi.org/10.1038/nature14338

Schuur, E. A. G., Abbott, B. W., Bowden, W. B., Brovkin, V., Camill, P., Canadell, J. G., et al. (2013). Expert assessment of vulnerability of permafrost carbon to climate change. *Climatic Change*, *119*(2), 359–374. https://doi.org/10.1007/s10584-013-0730-7

Schuur, E. A. G., Abbott, B. W., Commane, R., Ernakovich, J., Euskirchen, E., Hugelius, G., et al. (2022). Permafrost and climate change: Carbon cycle feedbacks from the warming Arctic. *Annual Review of Environment and Resources*, *47*(1), 343–371. https://doi.org/10.1146/annurev-environ-012220-011847

Serikova, S., Pokrovsky, O. S., Ala-Aho, P., Kazantsev, V., Kirpotin, S. N., Kopysov, S. G., et al. (2018). High riverine CO_2 emissions at the permafrost boundary of Western Siberia. *Nature Geoscience*, *11*(11), 825–829. https://doi.org/10.1038/s41561-018-0218-1

Tramontana, G., Jung, M., Schwalm, C. R., Ichii, K., Camps-Valls, G., Ráduly, B., et al. (2016). Predicting carbon dioxide and energy fluxes across global FLUXNET sites with regression algorithms. *Biogeosciences*, *13*(14), 4291–4313. https://doi.org/10.5194/bg-13-4291-2016

Treat, C. C., Bloom, A. A., & Marushchak, M. E. (2018). Nongrowing season methane emissions–a significant component of annual emissions across northern ecosystems. *Global Change Biology*, *24*(8), 3331–3343. https://doi.org/10.1111/gcb.14137

Turetsky, M. R., Abbott, B. W., Jones, M. C., Anthony, K. W., Olefeldt, D., Schuur, E. A. G., et al. (2020). Carbon release through abrupt permafrost thaw. *Nature Geoscience*, *13*(2), 138–143. https://doi.org/10.1038/s41561-019-0526-0

Valentini, R. (2003). EUROFLUX: An integrated network for studying the long-term responses of biospheric exchanges of carbon, water, and energy of European forests. In *Fluxes of carbon, water and energy of European forests* (pp. 1–8). https://doi.org/10.1007/978-3-662-05171-9_1

Virkkala, A. M., Aalto, J., Rogers, B. M., Tagesson, T., Treat, C. C., Natali, S. M., et al. (2021). Statistical upscaling of ecosystem CO2 fluxes across the terrestrial tundra and boreal domain: Regional patterns and uncertainties. *Global Change Biology*, *27*(17), 4040–4059. https://doi.org/10.1111/gcb.15659

Walker, D. A., Epstein, H. E., Jia, G. J., Balser, A., Copass, C., Edwards, E. J., et al. (2003). Phytomass, LAI, and NDVI in northern Alaska: Relationships to summer warmth, soil pH, plant functional types, and extrapolation to the circumpolar Arctic. *Journal of Geophysical Research*, *108*(D2), 8169. https://doi.org/10.1029/2001JD000986

Wang, S., Zhang, Y., Ju, W., Chen, J. M., Ciais, P., Cescatti, A., et al. (2020). Recent global decline of CO_2 fertilization effects on vegetation photosynthesis. *Science*, *370*(6522), 1295–1300. https://doi.org/10.1126/science.abb7772

Wang, S., Zhang, Y., Ju, W., Qiu, B., & Zhang, Z. (2021). Tracking the seasonal and inter-annual variations of global gross primary production during last four decades using satellite near-infrared reflectance data. *Science of the Total Environment*, *755*, 142569. https://doi.org/10.1016/j.scitotenv.2020.142569

Warner, D., Bond-Lamberty, B., Jian, J., Stell, E., & Vargas, R. (2019). Spatial predictions and associated uncertainty of annual soil respiration at the global scale. *Global Biogeochemical Cycles*, *33*(12), 1733–1745. https://doi.org/10.1111/gcb.15666

Watts, J. D., Farina, M., Kimball, J. S., Schiferl, L. D., Liu, Z., Arndt, K. A., et al. (2023). Carbon uptake in Eurasian boreal forests dominates the high-latitude net ecosystem carbon budget. *Global Change Biology*, *29*(7), 1870–1889. https://doi.org/10.1111/gcb.16553

Watts, J. D., Natali, S. M., Minions, C., Risk, D., Arndt, K., Zona, D., et al. (2021). Soil respiration strongly offsets carbon uptake in Alaska and Northwest Canada. *Environmental Research Letters*, *16*(8), 084051. https://doi.org/10.1088/1748-9326/ac1222

Wik, M., Varner, R. K., Anthony, K. W., MacIntyre, S., & Bastviken, D. (2016). Climate-sensitive northern lakes and ponds are critical components of methane release. *Nature Geoscience*, *9*(2), 99–105. https://doi.org/10.1038/ngeo2578

Wilkinson, S., Andersen, R., Moore, P., Davidson, S. J., Granath, G., & Waddington, J. (2023). Wildfire and degradation accelerate northern peatland carbon release. *Nature Climate Change*, *13*(5), 1–6. https://doi.org/10.1038/s41558-023-01657-w

Wutzler, T., Lucas-Moffat, A., Migliavacca, M., Knauer, J., Sickel, K., Šigut, L., et al. (2018). Basic and extensible post-processing of eddy covariance flux data with REddyProc. *Biogeosciences*, *15*(16), 5015–5030. https://doi.org/10.5194/bg-15-5015-2018

Xue, S.-Y., Xu, H. Y., Mu, C. C., Wu, T. H., Li, W. P., Zhang, W. X., et al. (2021). Changes in different land cover areas and NDVI values in northern latitudes from 1982 to 2015. *Advances in Climate Change Research*, *12*(4), 456–465. https://doi.org/10.1016/j.accre.2021.04.003

Yao, H., Peng, H., Hong, B., Guo, Q., Ding, H., Hong, Y., et al. (2022). Environmental controls on multi-scale dynamics of net carbon dioxide exchange from an alpine peatland on the eastern Qinghai-Tibet Plateau. *Frontiers in Plant Science*, *12*, 3198. https://doi.org/10.3389/fpls.2021.791343

Yuan, W., Luo, Y., Richardson, A. D., Oren, R., Luyssaert, S., Janssens, I. A., et al. (2009). Latitudinal patterns of magnitude and interannual variability in net ecosystem exchange regulated by biological and environmental variables. *Global Change Biology*, *15*(12), 2905–2920. https://doi.org/10.1111/j.1365-2486.2009.01870.x

Yumashev, D., Hope, C., Schaefer, K., Riemann-Campe, K., Iglesias-Suarez, F., Jafarov, E., et al. (2019). Climate policy implications of nonlinear decline of Arctic land permafrost and other cryosphere elements. *Nature Communications*, *10*(1), 1–11. https://doi.org/10.1038/s41467-019-09863-x

Zhuang, Q., Melillo, J. M., Sarofim, M. C., Kicklighter, D. W., McGuire, A. D., Felzer, B. S., et al. (2006). CO_2 and CH_4 exchanges between land ecosystems and the atmosphere in northern high latitudes over the 21st century. *Geophysical Research Letters*, *33*(17), L17403. https://doi.org/10.1029/2006GL026972

Zona, D., Gioli, B., Commane, R., Lindaas, J., Wofsy, S. C., Miller, C. E., et al. (2016). Cold season emissions dominate the Arctic tundra methane budget. *Proceedings of the National Academy of Sciences of the United States of America*, *113*(1), 40–45. https://doi.org/10.1073/pnas.1516017113